analytical chemistry

pubs.acs.org/ac Article

Naphthalimide Derivative-Functionalized Metal–Organic Framework for Highly Sensitive and Selective Determination of Aldehyde by Space Confinement-Induced Sensitivity Enhancement Effect

Xiuli Wang, Abudurexiti Rehman, Rong-mei Kong, Yuanyuan Cheng, Xiaoxia Tian, Maosheng Liang, Lingdong Zhang, Lian Xia,* and Fengli Qu*

Cite This: *Anal. Chem.* 2021, 93, 8219–8227 Read Online

ACCESS | Metrics & More | Article Recommendations | Supporting Information

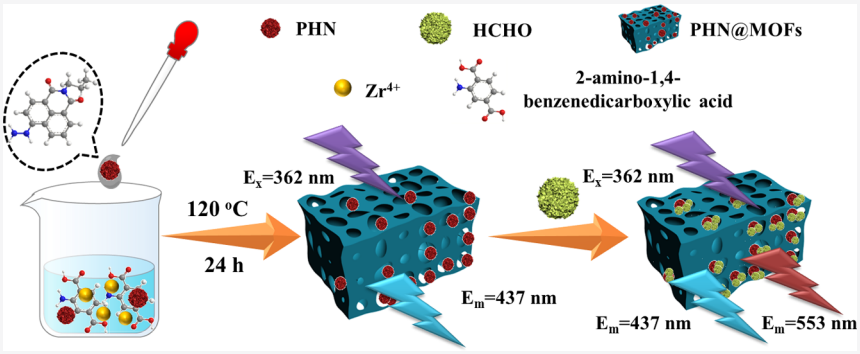

ABSTRACT: Facile and sensitive determination of formaldehyde (FA) in indoor environments still remains challenging. Herein, a fluorescent probe, termed PHN@MOF, was synthesized by embedding the fluorescent molecule of *N*-propyl-4-hydrazine-naphthalimide (PHN) into a metal–organic framework (MOF) for sensitive and visual monitoring of FA. The hydrazine group of PHN acts as the specific reaction group with FA based on the condensation reaction. The host of MOF (UiO-66-NH_2) offers the surrounding confinement space required for the reaction. Owing to the enrichment effect and molecular sieve selection of UiO-66-NH_2 to FA, PHN@MOF, compared with free PHN, exhibits very high sensitivity and selectivity based on space confinement-induced sensitivity enhancement (SCISE). Moreover, the fluorescence of UiO-66-NH_2 offers a reference signal for FA detection. Using this ratiometric fluorescent PHN@MOF probe, a colorimetric gel plate and test paper were developed and used to visually monitor FA in air.

Formaldehyde (FA), a familiar indoor air pollutant, is usually released from furniture, wood-based flooring, coating, insulation, textiles, and even cosmetic makeup, posing a significant threat to human health.[1,2] Long-term exposure to FA leads to such diseases as cancer, asthma, immune system disorders, and central nervous system damage.[3−5] Thus, severe FA exposure guidelines have been stipulated for indoor air by WHO (80 ppb) and different countries (e.g., 60 ppb by China).[6,7] This calls for effective and practical ways to monitor FA concentration in indoor environments, such as new homes, offices, and chemical factories.

At present, FA is usually detected by on-site sampling followed by off-site quantification in external analytical laboratories using sophisticated instruments (e.g., chromatography and mass spectrum). This procedure is time-consuming and labor-intensive.[8] Fortunately, chemical sensors show the potential for on-site monitoring with characteristics of simple application, miniaturization, and low consumption. Thus far, scientists have developed some satisfactory methods of FA detection, including electrochemical,[9,10] SERS,[11] fluorescence,[12,13] and polarographic determination.[14] While showing some success, the development of household FA detection sensors that can be used in surrounding air is still challenging by the limited portability. The characteristic of specific recognition of targets based on a specific reaction has resulted in the development of highly selective organic fluorescent probes for detecting FA in the last decades. Among these, two different kinds of fluorescence probes, including aza-Cope

Received: March 1, 2021
Accepted: May 19, 2021
Published: June 2, 2021

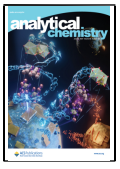

https://doi.org/10.1021/acs.analchem.1c00916
Anal. Chem. 2021, 93, 8219–8227

rearrangement-based[15,16] and aldehyde-amine condensation reaction-based probes,[17] have drawn interest in FA detection. Compared to aza-Cope rearrangement, the aldehyde-amine condensation reaction has shown more rapid reaction kinetics. Although various small-molecule probes have been developed for selective detection of FA based on these two mechanisms, their photobleaching resistance ability still needs to be improved.

Recently, space confinement-induced sensitivity enhancement (SCISE)[18,19] has attracted attention. SCISE occurs between porous host and guest and is based on target enrichment and the interference reduction. First, porous host nanomaterials adsorb target molecules into their pores through noncovalent interactions, such as H-bond and electrostatic adsorption.[20] If adsorption is based on specific interaction between functional groups of host and target molecules, selective enrichment should occur, thereby not only increasing the concentration of targets but also decreasing interference that concentrates around active sites. Therefore, the sensitivity of the probe can be substantially improved. Second, owing to the porous structure, the host material also shows the potential for molecular sieving, which can prevent bulky molecules from contact with a guest probe, thereby improving selectivity toward gas molecules of different sizes.

Many porous materials have been used as host materials of SCISE-based sensors, such as mesoporous silicon,[21,22] layered double hydroxide,[23,24] and metal−organic frameworks (MOFs).[25] Among these materials, MOFs, which are assembled from metal clusters and organic ligands, stand out as one kind of promising material owing to their unique properties.[26,27] The inherent characteristics of MOFs, such as highly specific surface area, ultrahigh porosity, large pore volume, tunable cage structures, and open metal sites, make them good candidates for providing a confined environment for the capture of guest molecules.[28−31] Compared with other MOFs, the amino-functionalized Zr-MOF of UiO-66-NH_2 not only shows high porosity, large surface area, and cage structure but also exhibits high chemical and thermal stability in both water and organic solvents. The pore size of UiO-66 was reported to be 11.5 Å,[32] whereas the window opening size was less than 6 Å.[33,34] Such a cage structure can block bulky molecules such as *o*-xylene (kinetic diameter around 7.4 Å)[35,36] from getting into the pores, thus decreasing interference based on size preference. The amino groups of UiO-66-NH_2 have a lone pair of electrons, which can easily adsorb targets with groups of electron acceptors,[37] resulting in the enhancement of preferential adsorption to FA. Moreover, the strong fluorescence emission at 450 nm of UiO-66-NH_2 allows the construction of ratiometric fluorescent probes. However, to the best of our knowledge, this kind of fluorescent probe for FA remains elusive.

Inspired by the advantages of the aldehyde-amine condensation reaction and SCISE, we herein synthesized fluorescent probe *N*-propyl-4-hydrazine-naphthalimide (PHN) and embedded it into UIO-66-NH_2 to obtain a nanocomposite (PHN@MOF), which was subsequently used to construct a household monitoring device for FA. The hydrazine group of PHN acts as the response site for FA based on the condensation reaction, which could react rapidly and generate a stable methylenehydrazine product. The fluorescence of PHN could be recovered because of the prohibition of fluorescent photoinduced electron transfer (PET) (Scheme 1).[38,39] The host of UiO-66-NH_2 can offer the surrounding space confinement that allows PHN to respond to FA, leading to higher sensitivity and selectivity for FA detection. Compared with free PHN, PHN@MOF showed enhanced sensitivity and selectivity to FA. Moreover, the intrinsic fluorescence emission of UiO-66-NH_2 can offer a reference signal for FA detection (Scheme 2). Using this ratiometric fluorescent probe, a colorimetric gel plate and test paper were further developed and successfully used to visualize and monitor FA in air and alcohol.

Scheme 1. Schematic Illustration of the PHN@MOF Probe for the Detection of FA

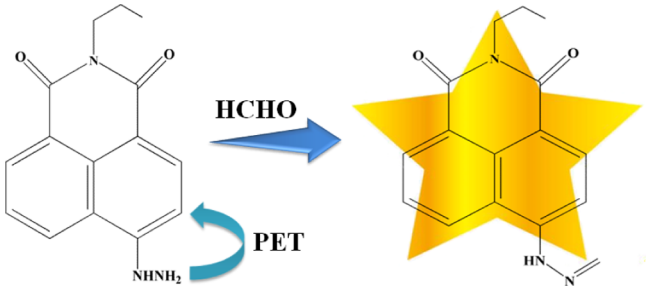

EXPERIMENTAL SECTION

Chemicals and Reagents. Propylamine was purchased from McLean Chemical Reagent Co., Ltd. Zirconium chloride was obtained from Shanghai Darui Fine Chemicals Co., Ltd. Benzoic acid was received from Tianjin Damao Chemical Reagent Factory. 2-Amino terephthalic acid was obtained from Shanghai Darui Fine Chemicals Co., Ltd. Hydrochloric acid was purchased from Jinan Reagent Factory. Hydrazine hydrate was obtained from Aladdin Chemistry Co., Ltd. 4-Bromine-1, 8-naphthalic anhydride was purchased from J&K Scientific Ltd. *N*,*N*-dimethylformamide (DMF) and ethanol were purchased from Sinopharm Chemical Reagent Co., Ltd. In addition, all other reagents and solvents were obtained commercially and used without further purification.

Instrumentation and Characterization. Transmission electron microscopy (TEM) measurements were performed on a JEOL 2010 microscope (JEOL 2010). Fourier transform infrared (FTIR) spectra were performed on a WQF-510A spectrophotometer in the range of 4000−500 cm^{-1}. Detection of UV−vis spectra was obtained using a UV752pc spectrophotometer. Fluorescence spectra were recorded using a Hitachi F-7000 fluorescence spectrophotometer. The ^1H NMR spectrum was obtained using a Bruker-500 MHz NMR (500 MHz/AVANCE III HD). High-performance liquid chromatography (HPLC) (Agilent, 1260) equipped with a fluorescent detector and C_{18} column (4.6 × 250 mm, 5 μm) was performed to obtain the HPLC data. X-ray photoelectron spectroscopy (XPS) analyses were carried out using an ESCALAB 250XI spectrometer. N_2 adsorption−desorption curves were obtained using a Kubox1000 specific surface area and an aperture analyzer. Mass spectrometry was performed on an Agilent 1290InfinityII/6564. Zeta potential was measured using Malvern Zen3600.

Preparation of UiO-66-NH_2 and PHN. According to the reported literature with slight modification,[40] the synthesis of UiO-66-NH_2 was performed by dissolving $ZrCl_4$ (0.1864 g), 2-amino-1,4-benzenedicarboxylic acid (0.1328 g), benzoic acid (1.4640 g), and hydrochloric acid (144 μL) into DMF (28 mL) with ultrasonic vibration for 15 min. Then, the resulting

https://doi.org/10.1021/acs.analchem.1c00916
Anal. Chem. 2021, 93, 8219−8227

Scheme 2. Schematic Illustration of the PHN@MOF Probe for the Detection of FA

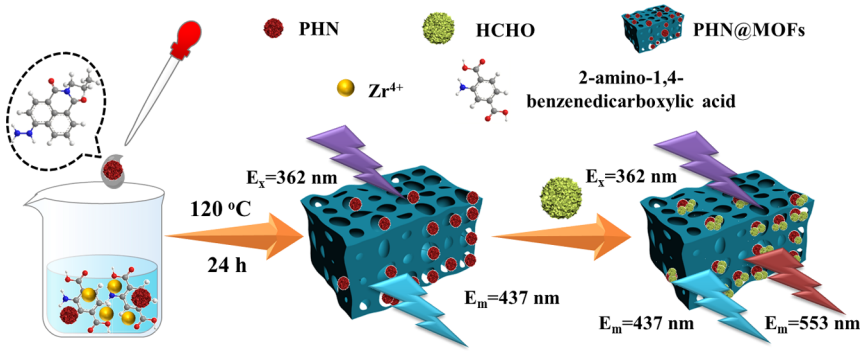

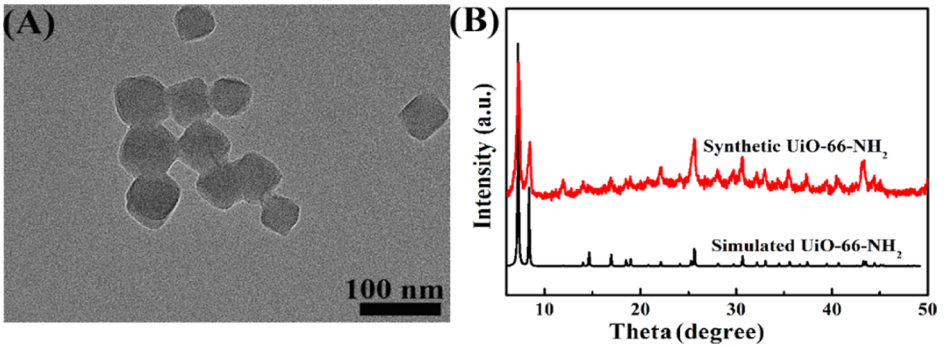

Figure 1. (A) TEM image of UiO-66-NH_2. (B) XRD of synthetic UiO-66-NH_2 (red) and simulated UiO-66-NH_2 (black).

mixture was placed into an oil bath and heated for 24 h at 393 K. After cooling to room temperature naturally, the precipitate was separated by centrifugation and then washed three times with DMF and ethanol, separately. After drying at 343 K under vacuum, the yellow powder product was harvested.

According to the reported literature with slight modification, the PHN product was prepared as follows:[41] ten mmol 4-bromine-1, 8-naphthalic anhydride, and 30 mmol propylamine were dissolved into 60 mL of ethanol. Then, the mixture was refluxed under 90 °C for 6 h to yield the condensate. After that, the resultant reaction solution was poured into 1000 mL of deionized water and then dewatered using a vacuum pump. The resultant intermediate product was redissolved into 80 mL of ethanol, and a condensation reaction was carried out at 90 °C for 8 h. One mmol hydrazine hydrate per hour was added into the mixture. The resultant mixture was poured into 1000 mL of deionized water and then dewatered using a vacuum pump. The product was dried at 333 K overnight.

^{1}H NMR (400 MHz, DMSO, d_6): δ 10.2 (3H, s, N−H), 7.63 (1H, d, Ar−H), 8.02 (1H, t, Ar−H), 8.24 (1H, d, Ar−H), 8.36 (1H, d, Ar−H), 8.59 (1H, d, Ar−H), 2.45 (2H, t,CH_2) 1.70 (2H, m, CH_2), 1.12 (3H, t, CH_3).

Preparation of PHN@MOF. PHN@MOF was synthesized using the same method as that for preparing UiO-66-NH_2 except that PHN (0.05 g) was added into the precursor solution of UiO-66-NH_2.

Fluorescence Sensing Experiment. One hundred μL of PHN@MOF suspension (300 μg/mL) and 100 μL of different concentrations of HCHO aqueous solution were added into 800 μL of Tris buffer (pH 6.4). The mixture was incubated for about 15 min at room temperature, followed by the measurement of the fluorescence spectrum. To evaluate the selectivity of PHN@MOF for FA detection, 100 μL of PHN@MOF suspension (300 μg/mL), 100 μL of different potential interferences (50 μM), including acetone, cysteine, aldehyde, H_2O_2, Ca^{2+}, Mg^{2+}, Na^+, Mn^{2+}, Co^{2+}, NO_3^-, Br^-, NO_2^-, SO_4^{2-}, I^-, Cl^-, methylbenzene, phenol, and resorcinol, and 800 μL of Tris buffer (pH 6.4) were mixed and incubated for 15 min at room temperature, followed by recording the fluorescence intensity.

Detection of FA in Liqueur and Air Samples. One hundred μL of PHN@MOF suspension (300 μg/mL), 100 μL of 10% liqueur, and 100 μL of different concentrations of HCHO were added into 700 μL of Tris buffer (pH 6.4). The mixture was reacted for about 15 min, and then, the fluorescence spectra were measured. The test paper was dipped in a vial containing PHN@MOF suspension (300 μg/mL) and dried in an oven at 40 °C. The process was repeated five times. FA detection in air samples: the test paper was hung in a 30 mL bottle containing a drop of 0.1 M methylbenzene, phenol, resorcinol, and FA, respectively, and the bottles were heated at 100 °C. Photographs of the test paper were taken after 15 min of response under a 365 nm UV light. The preparation process of silica gel plates was as follows: the silica gel plates were immersed in PHN@MOF dispersions (0.3 mg/mL) and then dried in an oven at 40 °C. The process was repeated three times. We wrote "QF" on the silica gel sheets using the solutions of water, cysteine, acetaldehyde, H_2O_2, Ca^{2+}, Mg^{2+}, Na^+, Mn^{2+}, Co^{2+}, NO_3^-, Br^-, NO_2^-, SO_4^{2-}, I^-, and Cl^- (100 μM) and FA (10 μM) as ink, respectively. Photographs of the silica gel plates were taken after 15 min of response under a 365 nm UV light.

RESULTS AND DISCUSSION

Characterization of PHN@MOF. The synthesis process of PHN is shown in Scheme S1. The successful synthesis of PHN was confirmed by mass spectrometry and 1H NMR. As shown in Figure S1, the resultant PHN produced an intense molecular

https://doi.org/10.1021/acs.analchem.1c00916
Anal. Chem. 2021, 93, 8219−8227

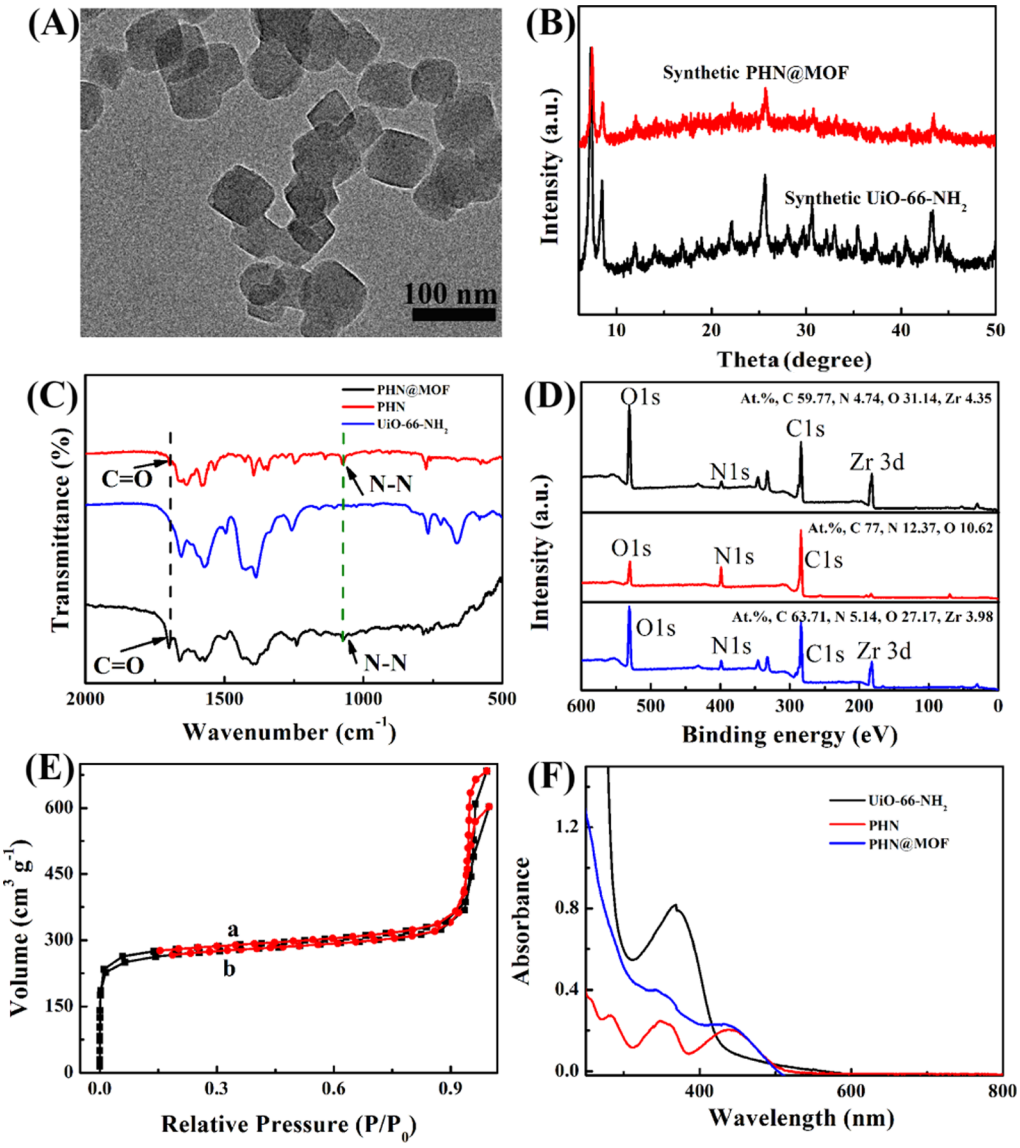

Figure 2. (A) TEM image of PHN@MOF. (B) XRD of UiO-66-NH_2 (black) and PHN@MOF (red). (C) FT-IR of UiO-66-NH_2 (blue), PHN (red), and PHN@MOF (black). (D) XPS spectra of UiO-66-NH_2 (black), PHN (red), and PHN@MOF (blue). (E) N_2 adsorption and desorption isotherms of UiO-66-NH_2 (a) and PHN@MOF (b). (F) UV−vis absorption spectra of UiO-66-NH_2 (black), PHN (red), and PHN@MOF (blue).

ion peak at m/z 269.6, which was consistent with the molecular weight of PHN,[41] together with the results of ^{1}H NMR, demonstrating that PHN had been successfully synthesized. The synthesis of UiO-66-NH_2 was characterized by SEM, TEM, and XRD. As shown in Figures S2 and 1A, we can see that the synthesized UiO-66-NH_2 exhibited an "octahedron-like" morphology with an average length of about 60 nm, which was consistent with that previously reported.[40] Figure 1B shows the XRD diffraction patterns of the synthesized UiO-66-NH_2, which highly matched those of the simulation,[42] suggesting that UiO-66-NH_2 had been successfully synthesized.

On the basis of the successful synthesis of PHN and UiO-66-NH_2, the PHN@MOF was then synthesized under the hydrothermal reaction and characterized. In order to investigate the influence of PHN load on the structure of UiO-66-NH_2, the morphology of PHN@MOF was first evaluated. As shown in Figures S3 and 2A, the structural morphology of the resultant PHN@MOF was the same as that of pristine UiO-66-NH_2, revealing that the loaded PHN caused no structural change in UiO-66-NH_2. From Figure 2B, we can see the XRD patterns of PHN@MOF, showing all peaks in the same positions as those of pristine UiO-66-NH_2, indicating that no contraction or change in the symmetry of the crystals happened as a result of the rigidity of UiO-66-NH_2. This suggested that the crystal structure of UiO-66-NH_2 had maintained the load of PHN molecules into its cavity. The FT-IR spectra comparing UiO-66-NH_2, PHN, and PHN@MOF are shown in Figure 2C. The absorption peaks at 1701 and 1069, which were derived from the C═O stretch vibration of dicarboximide and the N−N stretch vibration of hydrazine, were both observed in PHN and PHN@MOF, whereas pristine UiO-66-NH_2 did not show these characteristic absorption peaks.[43,44] Furthermore, XPS was used to verify the successful coupling of UiO-66-NH_2 with PHN molecules. Compared with PHN, Figure 2D shows that PHN@MOF had

https://doi.org/10.1021/acs.analchem.1c00916
Anal. Chem. 2021, 93, 8219−8227

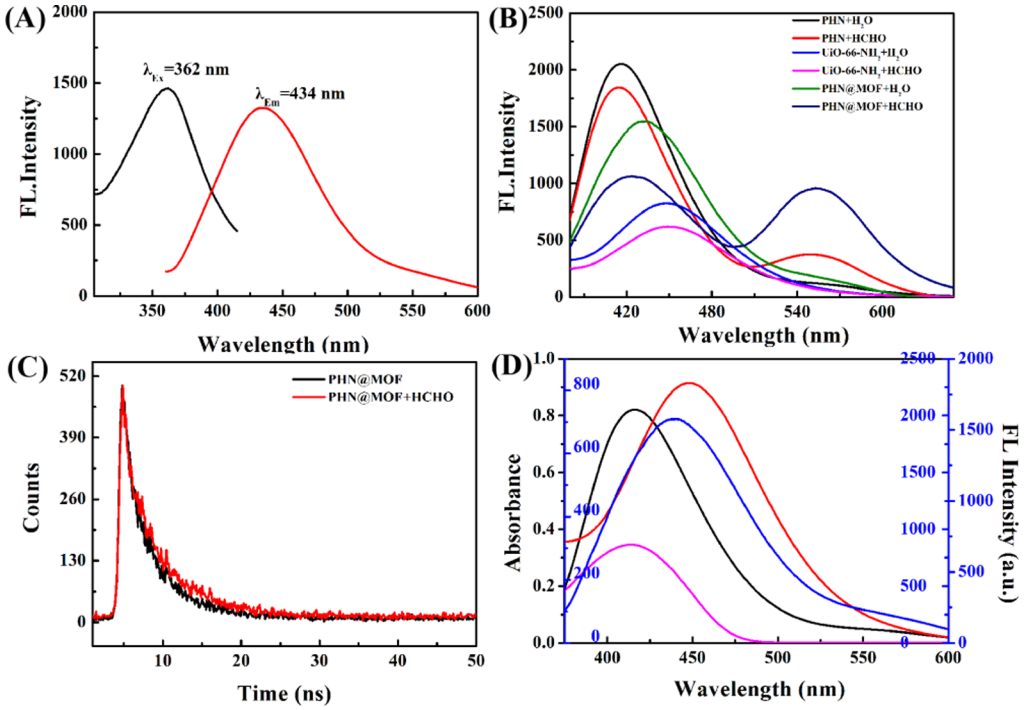

Figure 3. (A) Emission (Em) spectrum of PHN@MOF with λ_{Ex} = 362 nm (red); excitation (Ex) spectra of PHN@MOF with λ_{Em} = 434 nm (black). (B) Fluorescence emission spectra of PHN, UiO-66-NH_2, and PHN@MOF before and after the addition of 5 μM FA. (C) Time-resolved fluorescence decay profiles of the aqueous suspension of PHN@MOF before and after the addition of FA. (D) Emission spectra of PHN (black), UiO-66-NH_2 (red), and PHN@MOF (blue) and the UV−vis spectrum (pink) of HCHO (pink).

an additional peak at 185.22 and 183.02 eV, which could be attributed to Zr 3d.[45] Especially, the N and C percent in PHN@MOF was obviously higher than that in UiO-66-NH_2 after coupling with PHN, which further indicated the successful combination of PHN with MOF. In addition, the zeta potentials of UiO-66-NH_2, PHN, and PHN@MOF were obtained in Tris-HCl solution at room temperature (Table. S1). The results showed that the zeta potentials of UiO-66-NH_2 and PHN were about 38.8 and −29.9 mV, respectively.[46] Therefore, PHN molecules could combine with UiO-66-NH_2 tightly, according to the charge attraction, and suitable electrostatic repulsion could give rise to the homogeneous dispersion of PHN. As a result, the zeta potential of PHN@MOF (34.17 mV) fell between that of UiO-66-NH_2 and PHN after coupling. These results suggested that PHN had been successfully loaded into the cavity of UiO-66-NH_2 without any changes in the molecular structure.

The N_2 sorption−desorption isotherm was used to confirm the porosity of UiO-66-NH_2 and PHN@MOF. As shown in Figure 2E, the sorption−desorption processes of UiO-66-NH_2 and PHN@MOF were both classified as type-II isotherm, indicating that both UiO-66-NH_2 and PHN@MOF possessed a porous structure. The BET surface area and the pore value of the synthesized UiO-66-NH_2 and PHN@MOF were also measured by N_2 adsorption at 77 K. The results showed that the Brunauer, Emmett, and Teller (BET) surface area of UiO-66-NH_2 was 1034.8956 m^2/g[47] and that the pore size was 20 Å. After loading with PHN, the resultant PHN@MOF showed a slight decrease in the BET surface area and pore size, which were 923 m^2/g and 17 Å, respectively. These results indicated that crystal UiO-66-NH_2 had a large surface area and big pore size and that the load of PHN only had slight influence on these characteristics. Figure 2F shows the UV−vis absorption spectra of UiO-66-NH_2, PHN, and PHN@MOF. UiO-66-NH_2 (black) showed one absorption peak at 369 nm,[48] and PHN@MOF (blue) exhibited two absorption bands at 340 and 431 nm,[41] respectively, which largely resembled those of PHN (red).

Feasibility of PHN@MOF for Detecting FA. The fluorescence property of PHN@MOF was further investigated. Figure 3A demonstrates that PHN@MOF emits blue fluorescence centered at 434 nm upon excitation of 362 nm. In order to highlight the better performance of PHN@MOF, the fluorescence property of PHN, UiO-66-NH_2, and PHN@MOF before and after reacting with FA was investigated (Figure 3B). Under an excitation wavelength of 362 nm, the UiO-66-NH_2 nanoparticle showed a single fluorescence emission at 456 nm, which decreased slightly after being treated with FA. PHN exhibited a single emission at 417 nm in the absence of FA. However, after incubation with FA for 15 min, the fluorescence intensity at 417 nm showed a slight decrease, and a new fluorescence peak at 553 nm appeared. This is because the fluorescence at 553 nm of pristine PHN was initially suppressed by the PET effect between the hydrazine group and its chromophore. After reaction with FA, the PET effect was blocked by the formed hydrazone group, turning on fluorescence.[49−51] To further study the interaction of PHN@MOF and FA, time-resolved fluorescence decay experiments of PHN@MOF before and after the reaction with FA were performed. According to Figure 3C, we can see that the fluorescence lifetime of PHN@MOF obviously increased after the reaction with FA, which further confirmed the inhibition of the PET process between them. Here, PHN@MOF also showed a single emission at 434 nm in the absence of FA, resulting from the overlap of UiO-66-NH_2 emission at 456 nm and PHN emission at 417 nm. However, after reacting

https://doi.org/10.1021/acs.analchem.1c00916
Anal. Chem. 2021, 93, 8219−8227

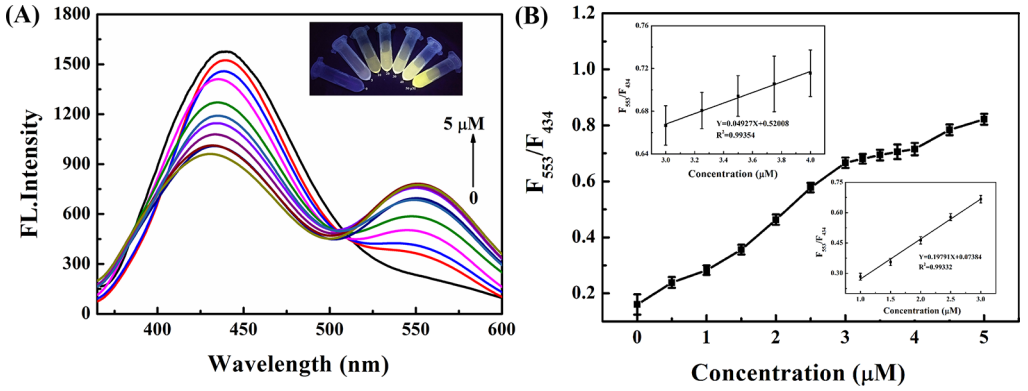

Figure 4. (A) Fluorescence spectra of the PHN@MOF probe in response to FA at varied concentrations (0−5 μM); inset: photographs of the sensing mixture with various concentrations (1−3 μM) of FA. (B) Fluorescence intensity ratio (F_{553}/F_{434}) of the PHN@MOF probe in response to FA.

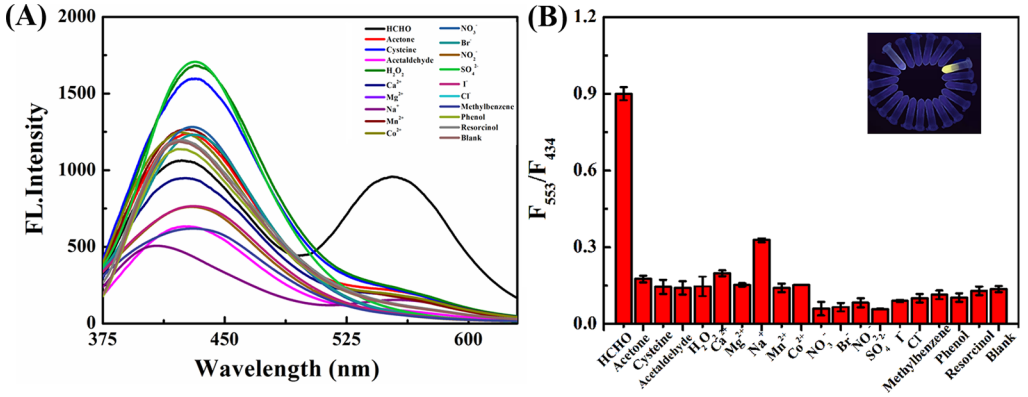

Figure 5. Selectivity of the sensing method against other interferences. Concentrations of FA and other interferences (acetone, cysteine, aldehyde, acetaldehyde, H_2O_2, Ca^{2+}, Mg^{2+}, Na^+, Mn^{2+}, Co^{2+}, NO_3^-, Br^-, NO_2^-, SO_4^{2-}, I^-, Cl^-, methylbenzene, phenol, and resorcinol) were 5 and 50 μM, respectively. (A) Fluorescence intensity spectra showing the response of the sensing system to different interferences. (B) Fluorescence intensity ratio (F_{553}/F_{434}) of the PHN@MOF probe toward various interferences. Inset: photographs at various interferences.

with FA, it was found that the fluorescence intensity of PHN@MOF initially decreased at 434 nm but then increased at 553 nm. The sensitivity of PHN@MOF to FA was much higher than that of PHN to FA. The reaction mechanism of PHN with FA, as shown in Schemes 1 and S2, was confirmed by HPLC (Figure S4) and HR-MS (Figure S5). As shown in Figure S4a, the retention time of PHN was 7.2 min. From Figure S4b, we can see that a new chromatographic peak at 5.8 min was observed after PHN reacting with FA, which we concluded to be the product of hydrazone. Then, HR-MS was performed to verify the product. From Figure S5, we can see that the molecular ion peak at m/z 282.3 was observed after PHN reacts with FA, which was consistent with the molecular weight of hydrazone. Therefore, after the reaction between PHN and FA, the resultant product of hydrazone was expected to be formed. In order to investigate why the reference signal decreased with increasing FA concentration, the UV−vis adsorption of PHN, UiO-66-NH_2, and PHN@MOF was detected, respectively. As shown in Figure 3D, the fluorescence emission spectra of PHN (black), UiO-66-NH_2 (red), and PHN@MOF (blue) considerably overlapped with the UV−vis absorption spectra of FA (black), indicating that the decrease in the reference signal at 434 nm could be attributed to the inner filter effect (IFE).[52] 3D emission profiles were then used to investigate the fluorescence properties of PHN@MOF. PHN@MOF exhibited maximum emission/excitation wavelengths at 434/362 nm (Figure S6A). However, after incubating with formaldehyde for 15 min, a new strong emission fluorescence peak at 553 nm appeared in the 3D emission of PHN@MOF (Figure S6B). To prove the stability of PHN@MOF for FA detection, the fluorescence intensity ratio at F_{553}/F_{434} was investigated at different times (Figure S7). The results showed that the fluorescence intensity ratio at F_{553}/F_{434} exhibited negligible change in 72 h. The morphology of PHN@MOF after the addition of FA was further investigated, and the results are shown in Figure S8. The SEM image (Figure S8A) and the TEM image (Figure S8B) show that the morphology of PHN@MOF after the addition of FA was the same as that of pristine PHN@MOF, revealing that incubation with FA did not cause structural collapse of PHN@MOF. Therefore, PHN@MOF can be employed as an ideal ratiometric probe for the detection of FA with excitation at 362 nm.

Performance of PHN@MOF for Detecting FA. To investigate the fluorescence titration of FA using PHN@MOF as the sensing platform, PHN@MOF water solution (0.3 mg/mL) was incubated with different concentrations of FA (0−5 μM) for 15 min at room temperature. The optimization process of the sensing condition is shown in Figure S9. Based on the data shown in Figure 4A, as FA concentration increased, the fluorescence intensity at 434 nm decreased, and the emission at 553 nm gradually increased. The inset of

https://doi.org/10.1021/acs.analchem.1c00916
Anal. Chem. 2021, 93, 8219−8227

Figure 4A shows the photograph of the sensing mixture with different FA concentrations under a UV light at 365 nm. With increasing FA concentration, results showed that the emission of the sensing mixture changed gradually from blue to bright yellow. Figure 4B shows that the fluorescence intensity ratio (F_{553}/F_{434}) of PHN@MOF had good linear relationships with FA concentration in the range of 1−3 and 3−4 μM (R^2 = 0.9933 and 0.9935). Based on the signal-to-noise ratio of S/N = 3, the limit of detection (LOD) was calculated to be 0.173 μM, which was lower than the LOD of PHN (3.2 μM). Compared to single PHN, PHN@MOF was more sensitive to FA by the SCISE of MOF host. Since UiO-66-NH_2 was rich with amine, the hydrogen bonds of amine could easily form with FA (Figure S10), facilitating surface adsorption. Therefore, local concentration of FA around the MOF increased, leading to higher response sensitivity. These results suggested that the established sensing platform presented a satisfactory fluorescence and naked-eye detection method for FA.

The selectivity of the PHN@MOF for FA was investigated by performing fluorescence tests in the presence of potential interference species, including acetone, cysteine, aldehyde, H_2O_2, Ca^{2+}, Mg^{2+}, Na^+, Mn^{2+}, Co^{2+}, NO_3^-, Br^-, NO_2^-, SO_4^{2-}, I^-, Cl^-, methylbenzene, phenol, and resorcinol (Figure 5). As shown in Figure 5A, the fluorescence emission at 553 nm is greatly enhanced after reacting with FA. However, even with 10 times concentration of FA, the interference species exhibit negligible fluorescence change at 553 nm. Figure 5B shows that the fluorescence intensity ratio (F_{553}/F_{434}) of PHN@MOF gives a remarkable increase with response to FA and negligible responses to interference species, which is highly consistent with Figure 5A, suggesting that PHN@MOF has high specific recognition of FA. Compared to the free PHN, the selectivity of PHN@MOF is better for the SCISE (Figure S11). The pore size of UiO-66-NH_2 synthesized in this work was determined to be 20 Å, whereas the window opening size is less than 6 Å, which permits the small molecules, such as FA, entering but blocks the bulky molecules, such as toluene and phenol, getting into the pores (Figure S12). Therefore, the PHN@MOF shows higher selectivity and sensitivity to FA than the free PHN.

Practical Application of PHN@MOF for Detecting FA. In order to study the practical applications of PHN@MOF for FA detection, a silica gel plate and filter paper were coated with PHN@MOF dispersive solution (0.3 mg/mL) as a test paper to detect FA. The letters "QF" were written on the silica gel plates using water, cysteine, acetaldehyde, H_2O_2, Ca^{2+}, Mg^{2+}, Na^+, Mn^{2+}, Co^{2+}, NO_3^-, Br^-, NO_2^-, SO_4^{2-}, I^-, and Cl^- (100 μM) and FA (10 μM) as ink, respectively. As shown in Figure 6, under UV light irradiation at 365 nm, no obvious changes were observed in the silica gel sheets written by interference species, while the script "QF" appears in yellow-green on the silica gel sheet coated in FA. In addition, a simulation of contaminated air was prepared by mixing air and benzenes, including methylbenzene, phenol, and resorcinol. This was used to further examine the practical ability of the developed test paper for FA monitoring. As shown in Figure 7, the air contaminated with FA reported out a remarkable change from blue to yellow, whereas the contaminated air without FA, but with interference species, showed no obvious color change. These results revealed that the developed test paper pretreated with PHN@MOF could be used as a satisfactory test strip for FA monitoring with characteristics of easy operation, high economy, high safety, and advanced efficiency.

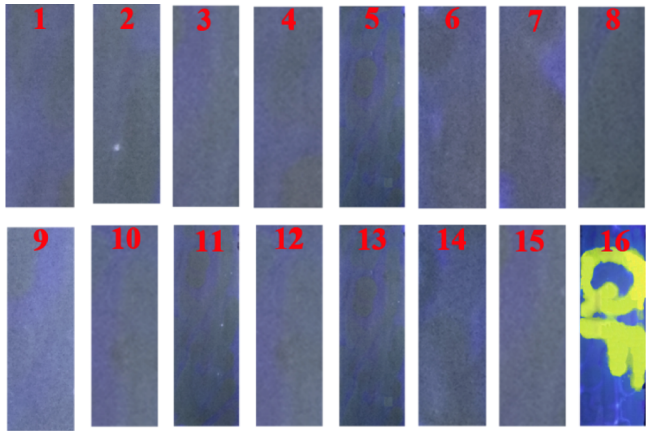

Figure 6. Photographs of silica gel plates under a 365 nm UV light upon coating with interferences (water, cysteine, acetaldehyde, H_2O_2, Ca^{2+}, Mg^{2+}, Na^+, Mn^{2+}, Co^{2+}, NO_3^-, Br^-, NO_2^-, SO_4^{2-}, I^-, and Cl^-) and FA. Concentrations of FA and other interferences (cysteine, acetaldehyde, H_2O_2, Ca^{2+}, Mg^{2+}, Na^+, Mn^{2+}, Co^{2+}, NO_3^-, Br^-, NO_2^-, SO_4^{2-}, I^-, and Cl^-) were 10 and 100 μM, respectively.

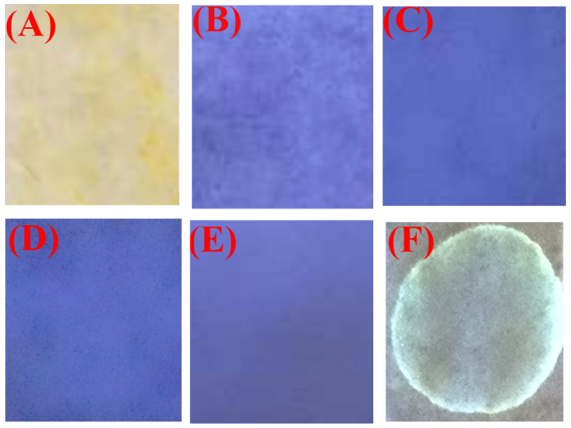

Figure 7. Photographs of the test paper under a visible light (A) and a 365 nm UV light. (B) Photographs of the test paper hanging upon 30 mL bottles containing contaminated air and methylbenzene (C), phenol (D), resorcinol (E), and FA (F) solutions (0.1 M), respectively, under a 365 nm UV light.

Practical Application. To further evaluate the feasibility of PHN@MOF as a sensor for practical FA detection, assay tests were carried out to detect FA in liqueur. The original samples were spiked with different concentrations of FA standards, followed by sensing performance. The experimental results are shown in Table 1. From Table 1, we can see that the recoveries of FA for all the samples with different concentrations range from 93.33 to 105.00% with RSD less than 5%. These results demonstrated that the PHN@MOF sensor had satisfactory accuracy and precision for detecting FA in liqueur.

Table 1. Recovery of 10% Liqueur Samples Containing Different Concentrations of FA Measured by Fluorescence Spectrometry

sample	added (μM)	found (μM)	recovery (%)	RSD (%, n = 3)
1	1.00	1.05	105.00	1.89
2	2.00	2.04	102.22	2.70
3	3.00	2.80	93.33	3.62

https://doi.org/10.1021/acs.analchem.1c00916
Anal. Chem. 2021, 93, 8219−8227

In order to highlight the application of the proposed method for detecting FA, the analysis parameters of FA detection with different methods were compared (Table S2). As shown in Table S2, the method proposed in this study had the advantages of simple design, low synthesis cost, high selectivity, low instrument price, and low LOD, when compared with methods reported in the previous literature.

CONCLUSIONS

In summary, a ratiometric fluorescent probe for FA sensing was successfully synthesized by embedding the fluorescent probe PHN into UiO-66-NH_2 through one-pot. The hydrazine group of PHN acts as the specific reaction group with FA based on the condensation reaction. The host of MOF (UiO-66-NH_2) offers surrounding space confinement for the reaction. Compared with free PHN, PHN@MOF with SCISE shows higher selectivity and sensitivity to FA, owing to the molecular sieve selection and enrichment effect of UiO-66-NH_2 for FA. The fluorescence emission of UiO-66-NH_2 also offers a reference signal for FA detection. Based on this ratiometric fluorescent probe, a simple method was developed and used for successful visual monitoring of FA in air and alcohol. The strategy of embedding guest recognition molecules into host porous nanomaterials to improve selectivity and sensitivity can provide prospective potential for monitoring trace targets in complex samples.

ASSOCIATED CONTENT

Supporting Information

The Supporting Information is available free of charge at https://pubs.acs.org/doi/10.1021/acs.analchem.1c00916.

Synthesis of the fluorescent formaldehyde probe PHN; illustration of the mechanism of the PHN reaction with FA; HRMS spectral analysis of PHN; SEM image of UiO-66-NH_2; SEM image of PHN@MOF, and so on (PDF)

AUTHOR INFORMATION

Corresponding Authors

Lian Xia − *Chemistry and Chemical Engineering College, Qufu Normal University, Qufu 273165, PR China;* orcid.org/0000-0001-6117-7596; Email: xialian01@163.com

Fengli Qu − *Chemistry and Chemical Engineering College, Qufu Normal University, Qufu 273165, PR China;* orcid.org/0000-0001-6311-3051; Phone: +86 537 4456301; Email: fengliquhn@hotmail.com; Fax: +86 537 4456301

Authors

Xiuli Wang − *Chemistry and Chemical Engineering College, Qufu Normal University, Qufu 273165, PR China*

Abudurexiti Rehman − *Chemistry and Chemical Engineering College, Qufu Normal University, Qufu 273165, PR China*

Rong-mei Kong − *Chemistry and Chemical Engineering College, Qufu Normal University, Qufu 273165, PR China*

Yuanyuan Cheng − *Chemistry and Chemical Engineering College, Qufu Normal University, Qufu 273165, PR China*

Xiaoxia Tian − *Chemistry and Chemical Engineering College, Qufu Normal University, Qufu 273165, PR China*

Maosheng Liang − *Chemistry and Chemical Engineering College, Qufu Normal University, Qufu 273165, PR China*

Lingdong Zhang − *Chemistry and Chemical Engineering College, Qufu Normal University, Qufu 273165, PR China*

Complete contact information is available at: https://pubs.acs.org/10.1021/acs.analchem.1c00916

Author Contributions

All authors have given approval to the final version of the manuscript.

Notes

The authors declare no competing financial interest.

ACKNOWLEDGMENTS

This work is supported by grants awarded by the National Natural Science Foundation of China (no. 21505084, 21775089, and 22074080), Changjiang Scholar Program of the Ministry of Education of China, Natural Science Foundation Projects of Shandong Province (ZR2020MB056), Key Research and Development Program of Shandong Province (no. 2017GSF19109), Innovation Project of Shandong Graduate Education (no. SDYY16091), Taishan Scholar Program of Shandong Province (tsqn201909106), and College Students Innovation and Entrepreneurship Training Project of Shandong Province (no. S201910446019).

REFERENCES

(1) Li, Y.; Chen, N.; Deng, D.; Xing, X.; Xiao, X.; Wang, Y. *Sens. Actuators, B* **2017**, *238*, 264−273.
(2) Salthammer, T. *Angew. Chem., Int. Ed.* **2013**, *52*, 3320−3327.
(3) Wang, X.; Si, Y.; Wang, J.; Ding, B.; Yu, J.; Al-Deyab, S. S. *Sens. Actuators, B* **2012**, *163*, 186−193.
(4) Kukkar, D.; Vellingiri, K.; Kaur, R.; Bhardwaj, S. K.; Deep, A.; Kim, K.-H. *Nano Res.* **2019**, *12*, 225−246.
(5) Wu, K.; Kong, X. Y.; Xiao, K.; Wei, Y.; Zhu, C.; Zhou, R.; Si, M.; Wang, J.; Zhang, Y.; Wen, L. *Adv. Funct. Mater.* **2019**, *29*, 1807953.
(6) Feng, L.; Musto, C. J.; Suslick, K. S. *J. Am. Chem. Soc.* **2010**, *132*, 4046−4047.
(7) Fu, J.; Zhang, L. *Anal. Chem.* **2018**, *90*, 8080−8085.
(8) Taprab, N.; Sameenoi, Y. *Anal. Chim. Acta* **2019**, *1069*, 66−72.
(9) Sun, J.; Sun, L.; Bai, S.; Fu, H.; Guo, J.; Feng, Y.; Luo, R.; Li, D.; Chen, A. *Sens. Actuators, B* **2019**, *285*, 291−301.
(10) Trafela, Š.; Zavašnik, J.; Šturm, S.; Rožman, K. Ž. *Electrochim. Acta* **2019**, *309*, 346−353.
(11) Lv, Z.-Y.; Mei, L.-P.; Chen, W.-Y.; Feng, J.-J.; Chen, J.-Y.; Wang, A.-J. *Sens. Actuators, B* **2014**, *201*, 92−99.
(12) Dou, K.; Chen, G.; Yu, F.; Liu, Y.; Chen, L.; Cao, Z.; Chen, T.; Li, Y.; You, J. *Chem. Sci.* **2017**, *8*, 7851−7861.
(13) Ma, Y.; Tang, Y.; Zhao, Y.; Lin, W. *Anal. Chem.* **2019**, *91*, 10723−10730.
(14) Septon, J. C.; Ku, J. C. *Am. Ind. Hyg. Assoc. J.* **1982**, *43*, 845−852.
(15) Brewer, T. F.; Chang, C. J. *J. Am. Chem. Soc.* **2015**, *137*, 10886−10889.
(16) Feng, X.; Wei, Q.; Li, S.; Wei, X.; Yang, X.; Song, Z.; Geng, B.; Li, Z.; Zhang, J.; Yan, M. *Sens. Actuators, B* **2021**, *330*, 129342.
(17) Bruemmer, K. J.; Brewer, T. F.; Chang, C. J. *Curr. Opin. Chem. Biol.* **2017**, *39*, 17−23.
(18) Trivedi, K.; Yuk, H.; Floresca, H. C.; Kim, M. J.; Hu, W. *Nano Lett.* **2011**, *11*, 1412−1417.
(19) Ning, Z.; Chen, Z.; Zhang, Q.; Yan, Y.; Qian, S.; Cao, Y.; Tian, H. *Adv. Funct. Mater.* **2007**, *17*, 3799−3807.
(20) Wu, Z.; Zhao, D. *Chem. Commun.* **2011**, *47*, 3332−3338.
(21) Ma, L.; Zhang, M.; Yang, A.; Wang, Q.; Qu, F.; Qu, F.; Kong, R.-M. *Analyst* **2018**, *143*, 5388−5394.
(22) Yu, Y.; Li, G.; Liu, J.; Yuan, D. *Chem. Eng. J.* **2020**, *401*, 126139.

(23) Tian, R.; Zhang, S.; Li, M.; Zhou, Y.; Lu, B.; Yan, D.; Wei, M.; Evans, D. G.; Duan, X. *Adv. Funct. Mater.* **2015**, *25*, 5006−5015.
(24) Song, L.; Shi, J.; Lu, J.; Lu, C. *Chem. Sci.* **2015**, *6*, 4846−4850.
(25) Ni, J.; Li, M.-Y.; Liu, Z.; Zhao, H.; Zhang, J.-J.; Liu, S.-Q.; Chen, J.; Duan, C.-Y.; Chen, L.-Y.; Song, X.-D.; Li, D. *ACS Appl. Mater. Interfaces* **2020**, *12*, 12043−12053.
(26) Wang, X.; Xiao, H.; Li, A.; Li, Z.; Liu, S.; Zhang, Q.; Gong, Y.; Zheng, L.; Zhu, Y.; Chen, C.; Wang, D.; Peng, Q.; Gu, L.; Han, X.; Li, J.; Li, Y. *J. Am. Chem. Soc.* **2018**, *140*, 15336−15341.
(27) Furukawa, H.; Cordova, K. E.; O'Keeffe, M.; Yaghi, O. M. *Science* **2013**, *341*, 1230444.
(28) Gu, Z.-Y.; Wang, G.; Yan, X.-P. *Anal. Chem.* **2010**, *82*, 1365−1370.
(29) Zhang, Z.; Huang, Y.; Ding, W.; Li, G. *Anal. Chem.* **2014**, *86*, 3533−3540.
(30) Yan, M.; Ye, J.; Zhu, Q.; Zhu, L.; Huang, J.; Yang, X. *Anal. Chem.* **2019**, *91*, 10156−10163.
(31) Xu, G.; Yamada, T.; Otsubo, K.; Sakaida, S.; Kitagawa, H. *J. Am. Chem. Soc.* **2012**, *134*, 16524−16527.
(32) Katz, M. J.; Brown, Z. J.; Colón, Y. J.; Siu, P. W.; Scheidt, K. A.; Snurr, R. Q.; Hupp, J. T.; Farha, O. K. *Chem. Commun.* **2013**, *49*, 9449−9451.
(33) Kandiah, M.; Usseglio, S.; Svelle, S.; Olsbye, U.; Lillerud, K. P.; Tilset, M. *J. Mater. Chem. A* **2010**, *20*, 9848−9851.
(34) Cavka, J. H.; Jakobsen, S.; Olsbye, U.; Guillou, N.; Lamberti, C.; Bordiga, S.; Lillerud, K. P. *J. Am. Chem. Soc.* **2008**, *130*, 13850−13851.
(35) Lennox, M. J.; Düren, T. *J. Phys. Chem. C* **2016**, *120*, 18651−18658.
(36) Chang, N.; Yan, X.-P. *J. Chromatogr. A* **2012**, *1257*, 116−124.
(37) Wang, K.; Gu, J.; Yin, N. *Ind. Eng. Chem. Res.* **2017**, *56*, 1880−1887.
(38) Bi, A.; Gao, T.; Cao, X.; Dong, J.; Liu, M.; Ding, N.; Liao, W.; Zeng, W. *Sens. Actuators, B* **2018**, *255*, 3292−3297.
(39) Tang, Y.; Kong, X.; Liu, Z.-R.; Xu, A.; Lin, W. *Anal. Chem.* **2016**, *88*, 9359−9363.
(40) Gao, X.; Cui, R.; Ji, G.; Liu, Z. *Nanoscale* **2018**, *10*, 6205−6211.
(41) Tang, Y.; Kong, X.; Xu, A.; Dong, B.; Lin, W. *Angew. Chem., Int. Ed.* **2016**, *128*, 3417−3420.
(42) Chen, Q.; He, Q.; Lv, M.; Xu, Y.; Yang, H.; Liu, X.; Wei, F. *Appl. Surf. Sci.* **2015**, *327*, 77−85.
(43) Johnston, C. T.; Bish, D. L.; Eckert, J.; Brown, L. A. *J. Phys. Chem. B* **2000**, *104*, 8080−8088.
(44) Quante, H.; Müllen, K. *Angew. Chem., Int. Ed.* **1995**, *34*, 1323−1325.
(45) Wu, T.; Yan, T.; Zhang, X.; Feng, Y.; Wei, D.; Sun, M.; Du, B.; Wei, Q. *Biosens. Bioelectron.* **2018**, *117*, 575−582.
(46) Du, X.-D.; Yi, X.-H.; Wang, P.; Zheng, W.; Deng, J.; Wang, C.-C. *Chem. Eng. J.* **2019**, *356*, 393−399.
(47) Garibay, S. J.; Cohen, S. M. *Chem. Commun.* **2010**, *46*, 7700−7702.
(48) Zhang, J.; Hu, Y.; Qin, J.; Yang, Z.; Fu, M. *Chem. Eng. J.* **2020**, *385*, 123814.
(49) Ge, H.; Liu, G.; Yin, R.; Sun, Z.; Chen, H.; Yu, L.; Su, P.; Sun, M.; Alamry, K. A.; Marwani, H. M.; Wang, S. *Microchem. J.* **2020**, *156*, 104793.
(50) Liu, C.; Cheng, A.-W.; Xia, X.-K.; Liu, Y.-F.; He, S.-W.; Guo, X.; Sun, J.-Y. *Anal. Methods* **2016**, *8*, 2764−2770.
(51) Nandi, S.; Sharma, E.; Trivedi, V.; Biswas, S. *Inorg. Chem.* **2018**, *57*, 15149−15157.
(52) Liu, H.; Li, M.; Xia, Y.; Ren, X. *ACS Appl. Mater. Interfaces* **2017**, *9*, 120−126.

https://doi.org/10.1021/acs.analchem.1c00916
Anal. Chem. 2021, 93, 8219−8227